Available online at www.sciencedirect.com
ScienceDirect
Applied Mathematical Modelling 33 (2009) 1479–1492
APPLIED MATHEMATICAL MODELLING
www.elsevier.com/locate/apm

Numerical simulation of thermal problems coupled with magnetohydrodynamic effects in aluminium cell ☆

Y. Safa *, M. Flueck, J. Rappaz

Institute of Analysis and Scientific Computing, École Polytechnique Fédérale de Lausanne, Station 8, 1015 Lausanne, Switzerland

Received 27 December 2006; received in revised form 4 February 2008; accepted 8 February 2008
Available online 29 February 2008

Abstract

A system of partial differential equations describing the thermal behavior of aluminium cell coupled with magnetohydrodynamic effects is numerically solved. The thermal model is considered as a two-phases Stefan problem which consists of a non-linear convection–diffusion heat equation with Joule effect as a source. The magnetohydrodynamic fields are governed by Navier–Stokes and by static Maxwell equations. A pseudo-evolutionary scheme (Chernoff) is used to obtain the stationary solution giving the temperature and the frozen layer profile for the simulation of the ledges in the cell. A numerical approximation using a finite element method is formulated to obtain the fluid velocity, electrical potential, magnetic induction and temperature. An iterative algorithm and 3-D numerical results are presented.

Keywords: Aluminium electrolysis; Chernoff scheme; Heat equation; Magnetohydrodynamics; Ledge; Solidification

1. Introduction

A phase changing problem motivated by the modelling of thermal problem coupled with magnetohydrodynamic effects in a reduction cell is studied. In a smelting cell operating with Hall–Héroult process, the metal part is produced by the electrolysis of aluminium oxide dissolved in a bath based on molten cryolite [1]. Various phenomena take place in such a cell for which a transverse section is schematically pictured in Fig. 1.

Running from the anodes through liquid aluminium and collector bars, the steady electric current spreads in the electrolytic bath. The important magnetic field generated by the currents carried to the alignment of cells, coupled with the currents running through the cells themselves gives rise to a field of Laplace forces which maintains a motion within these two conducting liquids. A magnetohydrodynamic interaction takes place in the cell. In the other hand a heating source is produced by the Joule effect due to the electric resistivity of the bath.

☆ Sponsors: Alcan-Pechiney Company and Swiss National Science Foundation; Grant No. 200020-101391.
* Corresponding author. Tel.: +41 22 379 23 66; fax: +41 22 379 22 05.
E-mail addresses: yasser.safa@epfl.ch, yasser.safa@obs.unige.ch (Y. Safa).

0307-904X/$ - see front matter © 2008 Elsevier Inc. All rights reserved.
doi:10.1016/j.apm.2008.02.011

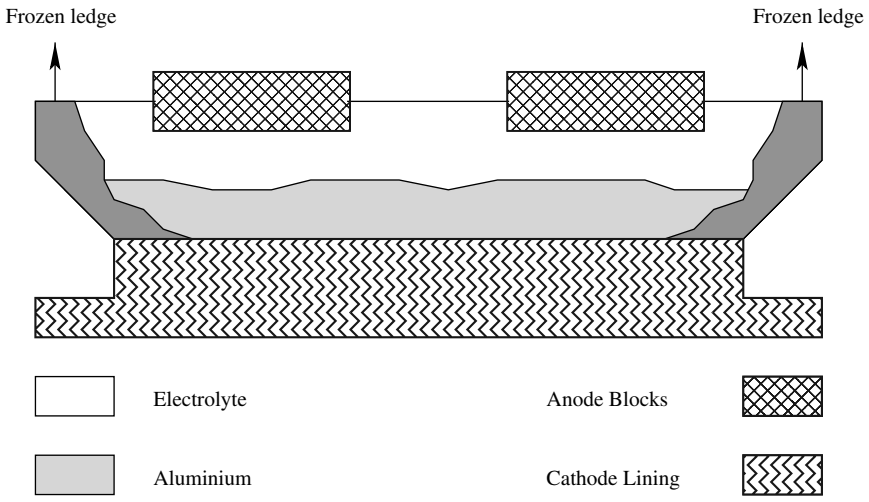

Fig. 1. Transverse cross section of aluminium reduction cell.

On the wall of the cell, a solidified bath layer, the so-called ledge is created. These ledges protect the cell sidewall from corrosive electrolytic bath and reduce the heat loss from the cell (see [2] page 23). Moreover, its profile strongly influences the magnetohydrodynamic stability causing oscillations of the aluminium–bath interface which could decrease the current efficiency. Consequently an optimal ledge profile is one of the objectives of cell sidewall design.

The thermal solidification problem in smelting cell has been treated by several authors [3–5]. As far as we are aware, this problem has never been considered when coupled with the magnetohydrodynamic fields. The aim of this paper is to deal with such fields interaction. Let us mention that the details on this problem can be found in Safa's thesis [6].

Mathematically, the problem is to solve a coupled system of partial differential equations consisting of the heat equation with Joule effect as a source, Maxwell law equations with electrical conductivity as a function of temperature and Navier–Stokes equations. The interface between aluminium and bath is an unknown. The ledge is considered as electrical insulator, the thermal model is a stationary two-phases Stefan problem. The outline of this paper is as follow: in Section 2 we introduce the physical model, the algorithm is presented in Section 3 and we give the numerical results in Section 4.

2. The model

In order to introduce the model we first describe some geometrical and physical quantities.

2.1. General descriptions

The geometry is schematically defined by Fig. 1. We introduce the following notations:

- $\Omega = \Omega_1 \cup \Omega_2$: fluids and solid ledge,
- $\Xi = \Xi_1 \cup \Xi_2$: electrodes,
- $\Lambda = \Omega \cup \Xi$: domain representing the cell

and we define the interfaces:

- $\Gamma = \partial\Omega_1 \cap \partial\Omega_2$: free interface between aluminium and bath, which is an unknown,
- $\Sigma_i = \partial\Lambda \cap \partial\Xi_i, \quad i = 1, 2,$
- $\Sigma = \Sigma_1 \cup \Sigma_2$: outer boundary of the electrodes.

The unknown physical fields with which we shall deal are listed as follows:
Hydrodynamic fields:

- $\boldsymbol{u}$: velocity field in $\Omega_i, i = 1, 2$, ($\boldsymbol{u} = 0$ in solid ledges),
- p: pressure.

Electromagnetic fields:

- $\boldsymbol{b}$: magnetic induction field,
- $\boldsymbol{e}$: electric field,
- $\boldsymbol{j}$: electric current density.

Thermal fields:

- H: enthalpy,
- θ: temperature.

The material properties are defined as

- ρ: mass density,
- σ_b and σ: electrical conductivity in and, respectively, outside the bath,
- η: viscosity of the fluids,
- μ_0: magnetic permeability of the void,
- k: thermal conductivity,
- C_p: specific heat,
- ℓ: latent heat.

2.2. Physical assumptions

The model leans on the following basic hypotheses:

1. The fluids are immiscible, incompressible and Newtonian.
2. In each domain Ω_i, $i = 1, 2$, the fluids are governed by the stationary Navier–Stokes equations.
3. The electromagnetic fields satisfy the stationary Maxwell's equations, Ohm's law is moreover supposed to be valid in all the cell Λ.
4. The electrical current density outside the cell is given (current in the collector bars).
5. The electrical conductivity σ is function of temperature θ in the fluids and electrodes parts.
6. The viscosity η, the density ρ and the specific heat C_p are temperature independent.
7. The volumes of the domains Ω_1 and Ω_2 have given values (mass conservation).
8. The only heat source is produced by the Joule effect due to the current crossing the cell.
9. Effects of chemical reactions [7], Marangoni effect [8,9], surface tension as well as the presence of gas flow are neglected.

2.3. The hydrodynamic problem

In this part we consider the temperature field θ and the electromagnetic fields $\boldsymbol{j}$ and $\boldsymbol{b}$ as known. We choose to represent the unknown interface between aluminium and bath by a parametrization of the form $\Gamma(\bar{h}) = [(x, y, z) : z = \bar{h}(x, y), (x, y) \in D]$, where D is usually a rectangle corresponding to the parametrization of aluminium–cathode interface. We denote the dependence of Ω_1, Ω_2 and Γ with respect to $\bar{h}$ by using

$$\Omega_i = \Omega_i(\bar{h}), \quad i = 1, 2, \quad \Gamma = \Gamma(\bar{h}).$$

From assumption (vii) we get the following relation:

$$\int_D \bar{h}(x,y)\,\mathrm{d}x\,\mathrm{d}y = V_1, \quad \text{where} \quad V_1 \text{ is the volume of aluminium.}$$

The unit normal to $\Gamma(\bar{h})$ pointing into $\Omega_2(\bar{h})$ is given by

$$\boldsymbol{n} = \frac{1}{\|\nabla(z-\bar{h})\|}\nabla(z-\bar{h}).$$

We consider the following standard set of equations for hydrodynamic fields:

$$\rho(\boldsymbol{u},\nabla)\boldsymbol{u} - \mathrm{div}(2\mu\mathbb{D}(\boldsymbol{u}) - (p+\rho gz)\mathbb{I}) = \boldsymbol{j}\wedge\boldsymbol{b} \qquad \text{in } \Omega_1(\bar{h})\cup\Omega_2(\bar{h}), \tag{1}$$

$$\mathrm{div}\boldsymbol{u} = 0 \qquad \text{in } \Omega_1(\bar{h})\cup\Omega_2(\bar{h}), \tag{2}$$

$$(\boldsymbol{u},\nabla(z-\bar{h})) = 0 \qquad \text{on } \Gamma(\bar{h}), \tag{3}$$

with

$$\mathbb{D}(\boldsymbol{u}) = \frac{1}{2}(\nabla\boldsymbol{u} + (\nabla\boldsymbol{u})^{\mathrm{T}}), \quad \mathbb{I} = (\delta_{ij}) \quad i,j = 1,2,3.$$

Here (.,.) is the usual scalar product on $\mathbb{R}^3$. Eqs. (1)–(3) correspond to 1st and 2nd assumptions. We complete those equations by introducing the conditions on the boundaries of the domains $\Omega_1(\bar{h})$ and $\Omega_2(\bar{h})$ containing the fluids. For any field w, $[w]_{\Gamma(\bar{h})}$ denotes the jump of w across $\Gamma(\bar{h})$, i.e. $[w]_{\Gamma(\bar{h})} = w_{\text{bath}} - w_{\text{aluminium}}$. For the fields $\boldsymbol{u}$ and p we have

$$\boldsymbol{u} = 0 \quad \text{on } \partial\Omega, \tag{4}$$

$$[\boldsymbol{u}]_{\Gamma(\bar{h})} = 0, \tag{5}$$

$$[(-p\mathbb{I} + 2\mu\mathbb{D}(\boldsymbol{u}))\boldsymbol{n}]_{\Gamma(\bar{h})} = 0. \tag{6}$$

The fluid part of $\Omega_i(\bar{h})$ $i = 1, 2$ is only a subdomain of the domain $\Omega_i(\bar{h})$ delimited by the front of solidification. In order to solve the hydrodynamic problem in a fixed domain Ω_i, we use the method of "fictitious domain" involving a penalization tool. The velocity and the pressure will then be defined in both liquids and solids. We add to Navier–Stokes equation the term $K(f_s)\boldsymbol{u}$, f_s is the solid fraction which is a function of temperature. The function K is given by "Carman Kozeny" law:

$$K(f_s) = \frac{\mu C f_s^2}{P^2(1-f_s)^3},$$

where P is the mean pore size and C is a constant obtained experimentally (see [10]). Eq. (1) may then be modified to

$$\rho(\boldsymbol{u},\nabla)\boldsymbol{u} - \mathrm{div}(2\mu\mathbb{D}(\boldsymbol{u}) - (p+\rho gz)\mathbb{I}) + K\boldsymbol{u} = \boldsymbol{j}\wedge\boldsymbol{b} \quad \text{in } \Omega_1(\bar{h})\cup\Omega_2(\bar{h}). \tag{7}$$

If only liquid phase is present we have $K = 0$ and the above equation reduces to the usual Navier–Stokes equation. Inside the mushy zone K may be very large, compared to the other terms, and the above equation mimics the Darcy law:

$$\nabla(p+\rho gz) = -K\boldsymbol{u} + \boldsymbol{j}\wedge\boldsymbol{b}.$$

When $f_s \to 1$, we get $K(f_s) \to \infty$ and then $\boldsymbol{u} = 0$ in the solid zone.

We finally obtain the hydrodynamic problem $\mathscr{P}_{\mathrm{HD}}$: for given $\boldsymbol{j}, \boldsymbol{b}$ and θ, find $\boldsymbol{u}$, p and $\bar{h}$ such that

$$\rho(\boldsymbol{u},\nabla)\boldsymbol{u} - \operatorname{div}(2\mu\mathbb{D}(\boldsymbol{u}) - (p+\rho g z)\mathbb{I}) + K\boldsymbol{u} = \boldsymbol{j}\wedge\boldsymbol{b} \qquad \text{in } \Omega_1(\bar{h})\cup\Omega_2(\bar{h}), \tag{8}$$

$$\operatorname{div}\boldsymbol{u} = 0 \qquad \text{in } \Omega_1(\bar{h})\cup\Omega_2(\bar{h}), \tag{9}$$

$$(\boldsymbol{u},\boldsymbol{n}) = 0 \qquad \text{on } \Gamma(\bar{h}), \tag{10}$$

$$\boldsymbol{u} = 0 \qquad \text{on } \partial\Omega, \tag{11}$$

$$[\boldsymbol{u}]_{\Gamma(\bar{h})} = 0, \tag{12}$$

$$[(-p\mathbb{I} + 2\mu\mathbb{D}(\boldsymbol{u}))\boldsymbol{n}]_{\Gamma(\bar{h})} = 0, \tag{13}$$

$$\int_D \bar{h}(x,y)\,\mathrm{d}x\,\mathrm{d}y = V_1. \tag{14}$$

2.4. The electromagnetic problem

We consider the velocity field $\boldsymbol{u}$ as well as the temperature θ are known. From the Faraday's law we have rot $\boldsymbol{e} = 0$, the electric field is then given by $\boldsymbol{e} = -\nabla\phi$, where ϕ is the electric potential field computed in Λ. We still denote by $\boldsymbol{u}$ the continuous extension of the velocity by zero in Λ, taking into account Ampere's law: rot $\boldsymbol{b} = \mu_0\boldsymbol{j}$ and Ohm's law: $\boldsymbol{j} = \sigma(-\nabla\phi + \boldsymbol{u}\wedge\boldsymbol{b})$ in Λ, we then obtain the electric conservation law given by

$$\operatorname{div}(-\sigma(\nabla\phi + \boldsymbol{u}\wedge\boldsymbol{b})) = 0 \quad \text{in } \Lambda.$$

We denote by $\frac{\partial}{\partial n}$ the operator $(\boldsymbol{n},\nabla)$, here $\boldsymbol{n}$ is the outer unit normal on $\partial\Lambda$.

We introduce the following boundary conditions concerning electric potential ϕ:

$$-\sigma\frac{\partial\phi}{\partial n} = 0 \qquad \text{on } \partial\Lambda\setminus\Sigma,$$

$$-\sigma\frac{\partial\phi}{\partial n} = j_0 \qquad \text{on } \Sigma_2,$$

$$\phi = 0 \qquad \text{on } \Sigma_1,$$

where j_0 is the given current density on the outer boundary of the anode Σ_2. Notice that magnetic induction $\boldsymbol{b}$ is obtained as a function of electrical current $\boldsymbol{j}$ by using Biot–Savart relation:

$$\boldsymbol{b}(\mathbf{x}) = \frac{\mu_0}{4\pi}\int_\Lambda \frac{\boldsymbol{j}(\mathbf{y})\wedge(\mathbf{x}-\mathbf{y})}{\|\mathbf{x}-\mathbf{y}\|^3}\,\mathrm{d}\mathbf{y} + \boldsymbol{b}_0(\mathbf{x}) \quad \forall\mathbf{x}\in\Lambda,$$

where $\boldsymbol{b}_0$ is some magnetic induction field due to the electric currents which flows outside the cell.

The electromagnetic problem $\mathscr{P}_{\mathrm{EM}}$ is then formulated as following: for given $\boldsymbol{u}$ and $\bar{h}$, find $\phi, \boldsymbol{b}$ and $\boldsymbol{j}$ such that

$$\operatorname{div}(\sigma(-\nabla\phi + \boldsymbol{u}\wedge\boldsymbol{b})) = 0 \quad \text{in } \Lambda, \tag{15}$$

$$-\sigma\frac{\partial\phi}{\partial n} = 0 \quad \text{on } \partial\Lambda\setminus\Sigma, \tag{16}$$

$$-\sigma\frac{\partial\phi}{\partial n} = j_0 \quad \text{on } \Sigma_2, \tag{17}$$

$$\phi = 0 \quad \text{on } \Sigma_1, \tag{18}$$

$$\boldsymbol{j} = \sigma(-\nabla\phi + \boldsymbol{u}\wedge\boldsymbol{b}) \quad \text{in } \Lambda, \tag{19}$$

$$\boldsymbol{b}(\mathbf{x}) = \frac{\mu_0}{4\pi}\int_\Lambda \frac{\boldsymbol{j}(\mathbf{y})\wedge(\mathbf{x}-\mathbf{y})}{\|\mathbf{x}-\mathbf{y}\|^3}\,\mathrm{d}\mathbf{y} + \boldsymbol{b}_0(\mathbf{x}) \quad \forall\mathbf{x}\in\Lambda. \tag{20}$$

2.5. The thermal problem

We consider as known the hydrodynamic field $\boldsymbol{u}$ and the electromagnetic field $\boldsymbol{j}$. The steady solution we are looking for will be here obtained as the limiting case of a time dependent heat equation.

In this subsection, we thus introduce the evolutionary thermal model. In our convection–diffusion problem the location of the front of solidification (interface separating ledge and liquid bath) is not known a priori and so needs to be determined as part of the solution. Such problems, widely referred as "Stefan problems", are highly non-linear. In order to overcome difficulty related to the non-linearity of the Stefan interface condition, an enthalpy function is defined, it represents the total heat content per unit volume of material. The enthalpy can be expressed in terms of the temperature, the latent heat ℓ and of the solid fraction f_s, namely:

$$H(\theta) = \int_0^\theta \rho C_p(s)\,\mathrm{d}s + \ell(1 - f_s(\theta)). \tag{21}$$

Since the enthalpy $H(\theta)$ is a monotonic function we can introduce the function β defined by the relation

$$\beta(H(\theta)) = \theta. \tag{22}$$

The function $\beta(H)$ is computed by mathematical processing (interpolation) in the list of (θ, H) values corresponding to the inverse relation $H = \beta^{-1}(\theta)$ given in Eq. (21). With this relation we can formulate the problem as a Stefan problem in temperature and enthalpy under the form

$$\frac{\partial H}{\partial t} - \mathrm{div}(k(\theta)\nabla\theta) + \rho C_p(\boldsymbol{u}, \nabla\theta) = \mathscr{S}, \tag{23}$$

$$\theta = \beta(H), \tag{24}$$

which is a non-linear convection–diffusion system. The term $(\boldsymbol{u}, \nabla\theta)$ denotes the scalar product of $\boldsymbol{u}$ with $\nabla\theta$, $\mathscr{S}$ is the heat source provided by Joule effect only. It takes the form

$$\mathscr{S} = \sigma\|\nabla\phi\|^2. \tag{25}$$

The advantage of this temperature–enthalpy formulation, taken in distributional sense, is that the necessity to carefully track the location of solid–liquid interface is removed and standard numerical technique can be employed to solve our phase change problem.

The temperature θ is subject to the Robin boundary condition:

$$k\frac{\partial\theta}{\partial n} = \alpha(\theta_a - \theta) \quad \text{on } \partial\Lambda, \tag{26}$$

where $\frac{\partial\theta}{\partial n}$ is the derivative in the direction of the outward unit normal on $\partial\Lambda$, α is the coefficient of thermal transfer, which may depends on both space and temperature, and θ_a is the temperature outside Λ. The heat transfer is due to convection and radiation. The radiation is implicitly taken into account by using:

$$\alpha = \alpha(\theta) = c_1 + c_2(\theta - c_3) \quad \mathrm{W/m^2\,{}^\circ C}$$

where c_1, c_2 and c_3 are positive values provided by experimental estimation.

An initial condition on enthalpy $H(\mathbf{x}, 0) = H_0$ on Λ is assumed.

For a given scalar value T, which will represent the integration time, we denote:

$$Q_T = \Lambda\times]0, T[\quad \text{and} \quad \Sigma_T = \partial\Lambda\times]0, T[.$$

The thermal problem $\mathscr{P}_{\mathrm{Th}}$ takes the form: for given $\boldsymbol{u}, \bar{h}$ and $\boldsymbol{j}$, find θ and H such that

$$\frac{\partial H}{\partial t} - \mathrm{div}(k(\theta)\nabla\theta) + \rho C_p(\boldsymbol{u}, \nabla\theta) = \mathscr{S} \quad \text{in } Q_T, \tag{27}$$

$$\theta = \beta(H) \quad \text{in } Q_T, \tag{28}$$

$$k(\theta)\frac{\partial\theta}{\partial n} = \alpha(\theta)(\theta_a - \theta) \quad \text{on } \Sigma_T, \tag{29}$$

$$H = H_0 \quad \text{in } \Lambda, \text{for } t = 0. \tag{30}$$

2.6. The full problem

We have just described the hydrodynamic, the electromagnetic and the thermal problems. In each of those we have assumed that the other fields were given.

The problem we want to solve is to find the velocity $\boldsymbol{u}$, the pressure p, the electrical potential ϕ, the enthalpy H and the temperature θ satisfying the three problems above; the functions $\beta(H), \alpha(\theta), C_{\mathrm{p}}(\theta), b_0(\mathbf{x}), H_0(\mathbf{x})$ and $f_{\mathrm{s}} = f_{\mathrm{s}}(\theta)$ are given and the constants $\rho, \mu_0, \ell, C_{\mathrm{p}}, \theta_{\mathrm{a}}, V_1, \sigma$ and μ are known.

3. The numerical approach

The numerical solution of the mathematical above problems is based on an iterative procedure in which we carry out alternatively the computation of the three types of unknowns: hydrodynamic *HD*, electromagnetic *EM* and thermic *Th*. In this section we present the iterative schemes for the problems $\mathscr{P}_{\mathrm{HD}}, \mathscr{P}_{\mathrm{EM}}$ and $\mathscr{P}_{\mathrm{Th}}$. A global "pseudo-evolutive" algorithm involving a space discretization by finite element method is applied for the solving of the three coupled problems.

3.1. Computation of the hydrodynamic fields

The hydrodynamic problem is iteratively solved. In each solving step, we first solve the problem in a fixed geometry without normal force equilibrium condition on the interface and then we update the interface position by using the non-equilibrium normal force. The solving deals with the alternative application of the two following steps:

- Step 1: we solve the hydrodynamic problem for the given geometry $\Gamma(\bar{h})$ and by taking into account the interface conditions:

  $$(\boldsymbol{u}, \boldsymbol{n}) = 0, \quad \text{on } \Gamma(\bar{h}),$$
  $$[((-p\mathbb{I} + 2\mu\mathbb{D}\boldsymbol{u})\boldsymbol{n}, \boldsymbol{t})]_{\Gamma(\bar{h})} = 0, \quad \forall\ \boldsymbol{t} \text{ tangential vector on } \Gamma(\bar{h}),$$

  the problem is then easily formulated on a weak formulation.
- Step 2: we update the position of interface in order to verify the equilibrium of normal forces on the interface Γ, we choose $\bar{h} := \bar{h} + \delta\bar{h}$ with:

$$\delta\bar{h} = -\frac{[((-p\mathbb{I} + 2\mu\mathbb{D}\boldsymbol{u})\boldsymbol{n}, \boldsymbol{n})]_{\Gamma(\bar{h})} + Cste}{[(\boldsymbol{j} \wedge \boldsymbol{b}, \boldsymbol{e}_z) - \rho g]_{\Gamma(\bar{h})}}.$$

Here we denote by $\boldsymbol{e}_z$ the unit vector of Oz axis and by *Cste* the constant obtained from the condition:

$$\int\int_D \delta\bar{h}(x, y)\,\mathrm{d}x\,\mathrm{d}y = 0.$$

An iterative scheme is used to compute $\boldsymbol{u}^{m+1}, p^{m+1}, Cste^{m+1}, \psi^{m+1}$ and $\bar{h}^{m+1}$ as functions of the values obtained from the previous iteration m.

We set $\psi = [((-p\mathbb{I} + 2\mu\mathbb{D}\boldsymbol{u})\boldsymbol{n}, \boldsymbol{n})]_{\Gamma(\bar{h})}$ and $f_z = (\boldsymbol{j} \wedge \boldsymbol{b}, \boldsymbol{e}_z) - \rho g$ and we define the solving step S^m_{HD} by

$$\rho(\boldsymbol{u}^m, \nabla)\boldsymbol{u}^{m+1} - \mathrm{div}(2\mu\mathbb{D}\boldsymbol{u}^{m+1} - (p^{m+1} + \rho g z)\mathbb{I}) + K\boldsymbol{u}^{m+1} = \boldsymbol{j}^m \wedge \boldsymbol{b}^m \quad \text{in } \Omega_1(\bar{h}^m) \cup \Omega_2(\bar{h}^m), \tag{31}$$

$$\mathrm{div}(\boldsymbol{u}^{m+1}) = 0 \quad \text{in } \Omega_1(\bar{h}^m) \cup \Omega_2(\bar{h}^m), \tag{32}$$

$$(\boldsymbol{u}^{m+1}, \boldsymbol{n}) = 0 \quad \text{on } \Gamma(\bar{h}^m), \tag{33}$$

$$[((-p^{m+1}\mathbb{I} + 2\mu\mathbb{D}\boldsymbol{u}^{m+1})\boldsymbol{n}, \boldsymbol{t})]_{\Gamma(\bar{h}^m)} = 0 \quad \forall\ \boldsymbol{t} \text{ tangent on } \Gamma(\bar{h}^m), \tag{34}$$

$$\psi^{m+1} = [((-p^{m+1}\mathbb{I} + 2\mu\mathbb{D}\boldsymbol{u}^{m+1})\boldsymbol{n}, \boldsymbol{n})]_{\Gamma(\bar{h}^m)}, \tag{35}$$

$$\bar{h}^{m+1} = \bar{h}^m - \frac{\psi^{m+1} + Cste^{m+1}}{[f_z^m]_{\Gamma(\bar{h}^m)}}, \tag{36}$$

$$_D(\bar{h}^{m+1} - \bar{h}^m)\,\mathrm{d}x\mathrm{d}y = 0. \tag{37}$$

Noting that the stop condition for this algorithm is based on H^1 norm estimation of $\boldsymbol{u}^{m+1} - \boldsymbol{u}^m$, which has to be smaller than a tolerance ϵ.

3.2. Computation of the electromagnetic fields

The magnetic induction $\boldsymbol{b}$ depends on electrical current $\boldsymbol{j}$ and implicitly on potential field ϕ, we have to compute the values of these electromagnetic fields for a known velocity field $\boldsymbol{u}^{m+1}$. To find ϕ we apply an iterative scheme in which, at the solving step m, we use the value of $\boldsymbol{b}^m$ to compute successively ϕ^{m+1} by using (15) and the boundary conditions (16)–(18) and then $\boldsymbol{j}^{m+1}$ by using (19). Subsequently, we apply Biot–Savart law to find the value of $\boldsymbol{b}^{m+1}$ as function of $\boldsymbol{j}^{m+1}$.

We carry out the solving step S^m_{EM} by

$$\operatorname{div}(-\sigma\nabla\phi^{m+1} + \sigma\boldsymbol{u}^{m+1} \wedge \boldsymbol{b}^m) = 0 \quad \text{in } \Lambda, \tag{38}$$

$$-\sigma\frac{\partial\phi^{m+1}}{\partial n} = 0 \quad \text{on } \partial\Lambda \setminus \Sigma, \tag{39}$$

$$-\sigma\frac{\partial\phi^{m+1}}{\partial n} = j_0 \quad \text{on } \Sigma_2, \tag{40}$$

$$\phi^{m+1} = 0 \quad \text{on } \Sigma_1, \tag{41}$$

$$\boldsymbol{j}^{m+1} = \sigma(-\nabla\phi^{m+1} + \boldsymbol{u}^{m+1} \wedge \boldsymbol{b}^m) \quad \text{in } \Lambda, \tag{42}$$

$$\boldsymbol{b}^{m+1}(\mathbf{x}) = \frac{\mu_0}{4\pi}\int_{\mathbb{R}^3} \frac{\boldsymbol{j}^{m+1}(\mathbf{y}) \wedge (\mathbf{x}-\mathbf{y})}{\|\mathbf{x}-\mathbf{y}\|^3}\,\mathrm{d}\mathbf{y} + \boldsymbol{b}_0(\mathbf{x}) \quad \forall\, \mathbf{x} \in \Lambda. \tag{43}$$

The stop condition is based on L^2 norm estimation of $\phi^{m+1} - \phi^m$ which has to be smaller than a tolerance ϵ.

3.3. Computation of the thermal fields

As already mentioned, we use a pseudo-evolutive description as a mathematical mean which converges toward the steady solution of thermal problem (27)–(30).

Making use of semi-implicit discretization in time of (27)–(30) we obtain

$$\frac{H^{m+1} - H^m}{\tau} - \nabla\cdot(k(\theta^m)\nabla\theta^{m+1}) + \rho C_{\mathrm{p}}(\boldsymbol{u}^m, \nabla\theta^{m+1}) = \mathscr{S}^m, \tag{44}$$

where H^m, θ^m and $\mathscr{S}^m$ are the values of H, θ and $\mathscr{S}$ at time $t^m = mtau$ and τ is the time step discretization. In order to close the system (44), we make use of the Chernoff scheme, namely

$$H^{m+1} = H^m + \gamma(\theta^{m+1} - \beta(H^m)), \tag{45}$$

where γ is a positive relaxation parameter. By replacing (45) in (44), we obtain a scheme in order to compute the temperature at time t_{n+1}, i.e.

$$\gamma\frac{\theta^{m+1} - \beta(H^m)}{\tau} - \nabla\cdot(k(\theta^m)\nabla\theta^{m+1}) + \rho C_{\mathrm{p}}(\boldsymbol{u}^{m+1}, \nabla\theta^{m+1}) = \mathscr{S}^m. \tag{46}$$

It is shown in [11] that the scheme is stable as long as γ satisfies the following condition:

$$0 < \gamma \leqslant \frac{1}{\sup_{s\in\mathbb{R}}\frac{\partial\beta(s)}{\partial s}}.$$

In the above equalities, θ^{m+1} is not a good value of the temperature in the mushy zone at time t^{m+1}, the good value for the temperature is obtained from $\beta(H^{m+1})$. In order to avoid a possible confusion, the first one will be

denoted by $\tilde{\theta}$. In time discretization form, we assume that we know H^m at the time step ($t^m = m\tau$), and we compute $\tilde{\theta}^{m+1}, H^{m+1}$ and θ^{m+1} at the solving step S^m_{Th} with the following scheme:

$$\gamma \frac{\tilde{\theta}^{m+1} - \beta(H^m)}{\tau} - \mathrm{div}(k(\theta^m)\nabla\tilde{\theta}^{m+1}) + \rho C_{\mathrm{p}}(\boldsymbol{u}^{m+1}, \nabla\tilde{\theta}^{m+1}) = \mathscr{S}^m \quad \text{in } \Lambda, \tag{47}$$

$$k(\theta^m)\frac{\partial\tilde{\theta}^{m+1}}{\partial n} = \alpha(\theta^m)(\theta_a - \tilde{\theta}^{m+1}) \quad \text{on } \partial\Lambda, \tag{48}$$

$$H^{m+1} = H^m + \gamma(\tilde{\theta}^{m+1} - \beta(H^m)) \quad \text{in } \Lambda, \tag{49}$$

$$\theta^{m+1} = \beta(H^{m+1}) \quad \text{in } \Lambda. \tag{50}$$

3.4. A Galerkin formulation

The three sets of equations $S^m_{\mathrm{HD}}, S^m_{\mathrm{EM}}$ and S^m_{Th} are numerically solved by a Galerkin formulation suited for a finite element approach with piecewise polynomials of degree one on a tetrahedron mesh. Fig. 2 shows the tetrahedron mesh $\mathscr{T}_h$ used for the computation.

Navier–Stokes Problem S^m_{HD} is numerically solved by using classical stabilised finite element method $\mathbb{P}_1$ (see [12]) and the potential problem S^m_{EM} by a standard finite element method with piecewise polynomials of degree 1. In this part we choose to focus our attention on the finite element approach corresponding to the thermal problem. Taking into account the value of local Peclet number (around 1000 in our case), we are using SUPG stabilization method (Streamline Upwind Petrov Galerkin) [13]. We define the finite element space

$$Y^{\mathrm{Th}}_h = \{\varphi \in C^0(\overline{\Lambda}); \forall\, K \in \mathscr{T}_h\},$$

where $\mathscr{T}_h$ denotes a mesh overlapping Λ with tetrahedrons K. The finite element formulation corresponding to the set of Eqs. (47)–(50) is given by: find $(\tilde{\theta}^{m+1}_h, \theta^{m+1}_h, H^{m+1}_h) \in (Y^{\mathrm{Th}}_h)^3$ such that

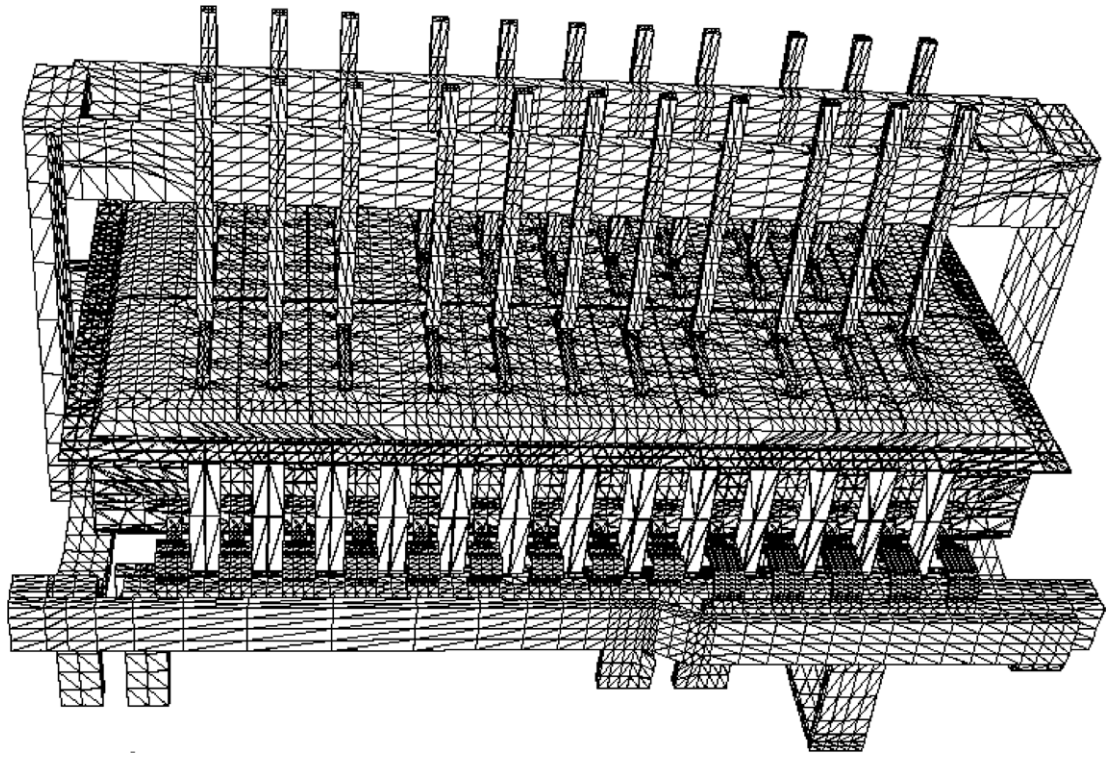

Fig. 2. The tetrahedron mesh of the domain.

$$\int_{\Lambda}\gamma\frac{\tilde{\theta}_h^{m+1}-\beta(H_h^m)}{\tau}\varphi_h\,\mathrm{d}\mathbf{x}+\int_{\Lambda}k^m(\nabla\tilde{\theta}_h^{m+1},\nabla\varphi_h)\,\mathrm{d}\mathbf{x}-\int_{\partial\Lambda}\alpha^m(\theta_a-\tilde{\theta}_h^{m+1})\varphi_h\,\mathrm{d}\Sigma$$
$$+\int_{\Lambda}\rho C_{\mathrm{p}}(\boldsymbol{u}^{m+1},\nabla\tilde{\theta}_h^{m+1})\varphi_h\,\mathrm{d}\mathbf{x}$$
$$+\sum_{K\in\mathscr{T}_h}\int_K\zeta_K\left(\gamma\frac{\tilde{\theta}_h^{m+1}-\beta(H_h^m)}{\tau}+\rho C_{\mathrm{p}}(\boldsymbol{u}^{m+1},\nabla\tilde{\theta}_h^{m+1})\right)(\boldsymbol{u}^{m+1},\nabla\varphi_h)\,\mathrm{d}\mathbf{x}$$
$$+\sum_{K\in\mathscr{T}_h}C_2\int_K\rho C_{\mathrm{p}}\delta_K h_K\|\boldsymbol{u}^{m+1}\|(\nabla\tilde{\theta}_h^{m+1},\nabla\varphi_h)\,\mathrm{d}\mathbf{x}$$
$$=\int_{\Lambda}\mathscr{S}^m\varphi_h\,\mathrm{d}\mathbf{x}+\sum_{K\in\mathscr{T}_h}\int_K\zeta_K\mathscr{S}^m(\boldsymbol{u}^{m+1},\nabla\varphi_h)\,\mathrm{d}\mathbf{x}\quad\forall\ \varphi_h\in Y_h^{\mathrm{Th}},\tag{51}$$

$$H_h^{m+1}=H_h^m+\gamma(\tilde{\theta}_h^{m+1}-r_h\beta(H_h^m))\quad\text{in }\Lambda,\tag{52}$$

$$\theta_h^{m+1}=r_h\beta(H_h^{m+1})\quad\text{in }\Lambda,\tag{53}$$

where r_h denotes the interpolant on the grid $\mathscr{T}_h$ and ζ_K is given by

$$\zeta_K=\begin{cases}C_1\frac{\delta_K h_K}{\|\boldsymbol{u}^{m+1}\|} & \text{if } \|\boldsymbol{u}^{m+1}\|>0,\\ 0 & \text{if } \|\boldsymbol{u}^{m+1}\|=0\end{cases}\tag{54}$$

with δ_K is

$$\delta_K=\begin{cases}Pe_K & \text{if } Pe_K<1,\\ 1 & \text{if } Pe_K\geqslant 1,\end{cases}\tag{55}$$

and h_K is the size of K, the term Pe_K is the local Peclet number. We denote by $k^m=k(\theta_h^m)$ and $\alpha^m=\alpha(\theta_h^m)$, respectively, the thermal conductivity and the heat transfer coefficient at time step m.

Remark. It is obvious that the enthalpy H has a jump on the solidification front which is not a priori known, but we approach H by H_h^{m+1} which is in the subspaces of continuous functions. Thus the approximation presents a strong gradient in a narrow region where the exact enthalpy makes a jump. In spit the fact that our discrete problem is well posed, we note that the convergence of the enthalpy approximation toward the solution H is only true in $L^2(\Lambda)$ norm.

4. Numerical results

We use GMRES to solve the matrix system resulting from the hydrodynamic problem (S_{HD}^m) and from the thermal problem (S_{Th}^m). In the other hand, since the matrix system related to the computation of electrical fields (S_{EM}^m) is symmetric positive definite, we use the Algebraic Multi Grid method AMG or the Conjugated Gradient method CG to solve this problem.

The MHD-Thermal calculation is carried out by using (PC Pentium(R) 4, CPU 2.80 GHz, 2 GB RAM) and the convergence of the global algorithm is obtained in 10 hours. The results relative to the computation of the electric potential are presented in Fig. 3. Fig. 4 shows the distribution of the temperature through the cell. The shape of the ledge is given in Fig. 5. We observe clearly the effect of numerical diffusion related to SUPG stabilization on the narrow region of the solidification's front. It may be worth pointing out the agreement of this picture with the one representing the velocity field (Fig. 6) and to notice in particular that the locations where this field is small correspond to the locations where the ledge is large.

It is easy to observe that the numerical results of the velocity field computations match Darcy law on the part of domain where the liquid fraction is less than 1. This shows the efficiency of using the method of "auxiliary domain" involving a penalization of the velocity field in the hydrodynamic model.

The fluid layer along their depth is discretized with several elements to have more accurate representation of hydrodynamic field. Further, as mentioned before, the nodes at interface aluminium–bath are allowed to move

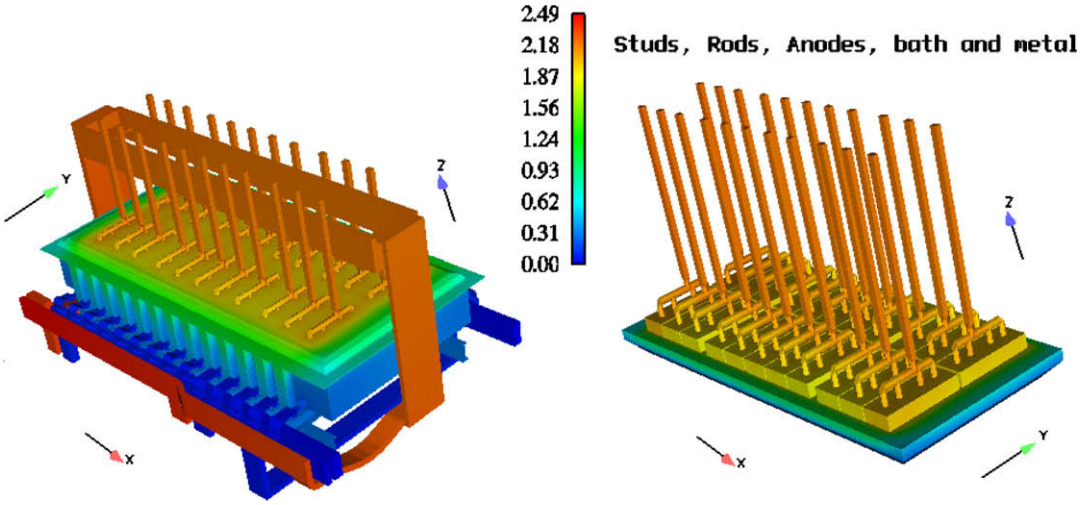

Fig. 3. Electric potential results in the cell.

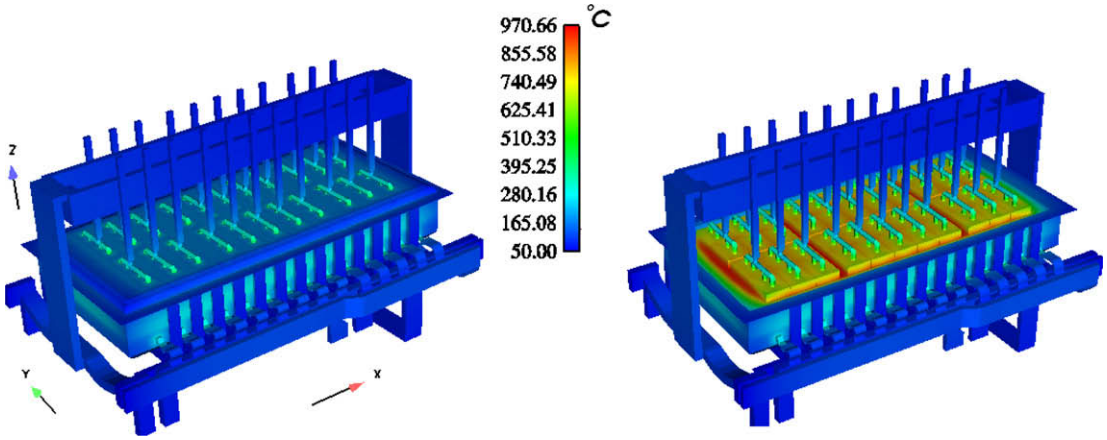

Fig. 4. Temperature results in the cell.

along vertical line to insure the vertical force equilibrium (Step 2 in the Section 3.1). The main value of error with respect to the liquid depth is 6%. At the level of aluminium–bath interface we have the highest convection effects and consequently the finest thickness of the ledge see Fig. 5

It is important to insure that the total heat dissipation matches the internal heat generation.It is critical that this is achieved in order to consider the results are corresponding to cell steady-state conditions. The total heat dissipation is obtained from the sum of Joule heat produced in each part Λ_j, $j = 1, \ldots, N$, where N is the number of the parts of the cell traversed by the electrical current:

$$\text{total heat dissipation} = \sum_{j=1}^{N} \int_{\Lambda_j} \sigma \|\nabla \phi\|^2 \, \mathrm{d}\mathbf{x} = 408.50 \text{ kW}.$$

The total heat lost corresponds to convective dissipation on the cells boundary $\partial\Lambda$:

$$\int_{\partial\Lambda} \alpha(\theta_a - \theta) \, \mathrm{d}\Gamma = 398.3 \text{ kW}.$$

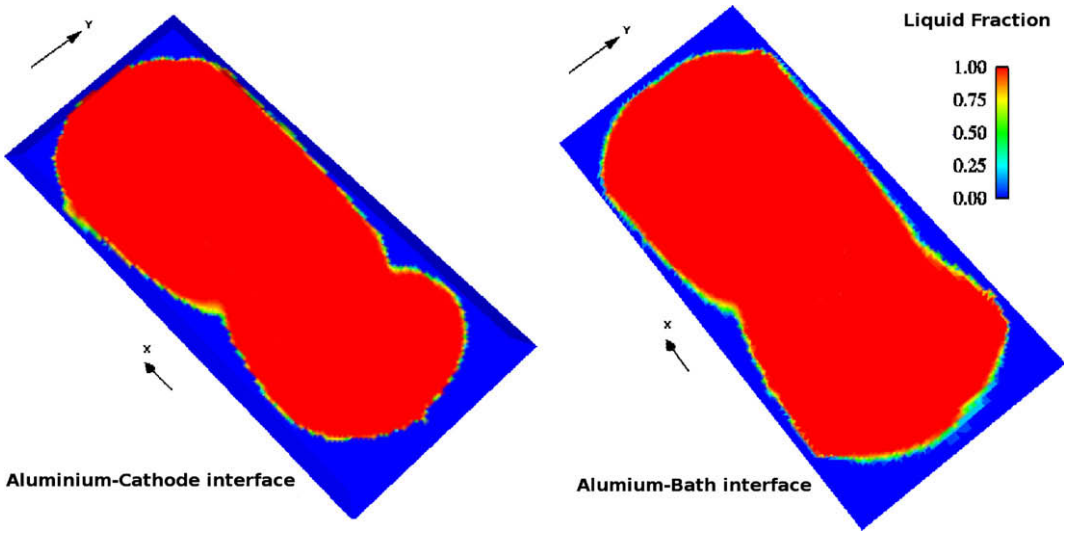

Fig. 5. Liquid fraction showing the ledge.

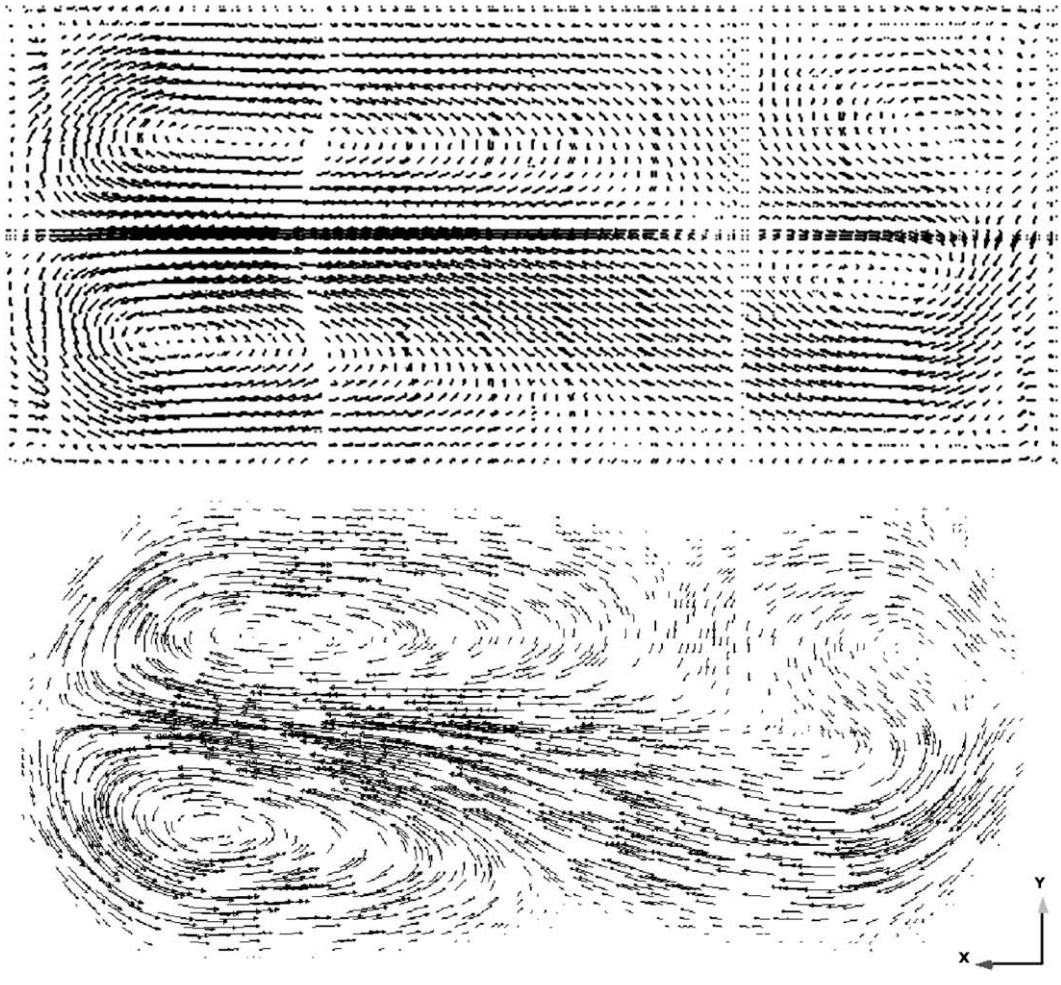

Fig. 6. Velocity field shown before solidification (above) and after solidification (below) wtih mean value = 0.8 cm/s.

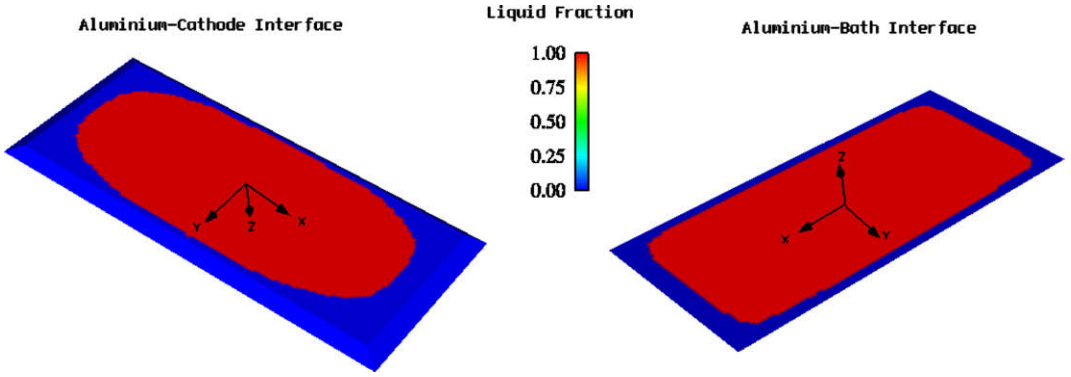

Fig. 7. Liquid fraction showing the ledge shape, electro-thermal computing.

The numerical error relative to total Joule dissipation is 2.5%. This value corresponds to the error resulting from the electro-thermal computation applied by using ANSYS code in a slice part of the cell, see [14].

An other approach was used to obtain the ledge shape. It leans on an electro-thermal computation without velocity field. The convection effects is simulated by using an artificial thermal conductivity in the metal-bath zone. A symmetric ledge is then obtained as shown in Fig. 7, compared with Fig. 5, it should be easy to observe the effects of velocity fields in the configuration of frozen ledge.

5. Conclusions

This work is in the prolongation of the former studies ([15,16]) intended for the derivation of criteria making it possible to determine the stable or unstable character movement of the fluids in a Hall–Héroult cell.

In the reference mentioned above these criteria come from an analysis in frequencies of the equations of the MHD, linearized around a stationary solution. It arises from the numerical studies carried out in [15] and in [16] that stability of these criteria rests, to a large extent, on the precision with which this stationary solution is obtained. By precision we understand here not only that related to a correct numerical approach but also that relating to the adequacy between the model and the description of the characteristics of the cell (see [17,18]).

In this paper the effects of the temperature distribution on the shape of the ledge and on the velocity field have been considered.

From the observations of the above results, the following conclusions were given:

the effects of hydrodynamic field is shown as an important factor which determines the thermal behavior of electrolysis cell. From Figs. 5 and 7 respectively, we see that the velocity field has a strong effect on the ledge shape.

The calculation is done without taking into account the erosion effect of hydrodynamic stress tensor on the ledge. This problem should be handled in the future.

In spite of the difficulty of multi-fields interactions and the complexity of geometrical conditions, the Chernoff scheme is stable in the resolution of thermomagnetohydrodynamic problem.

Finally we note that the study of thermo-mechanical deformation of steel shell of Aluminium reduction cell under the effect thermal expansion was handled by several authors [19–21]. The thermal computing in such works was never been coupled with hydrodynamic fields. The calculations of thermal fields shown in this paper are fruitful for an elasto-thermal computing achieved later by Safa and al. in [22] in order to show the effects of thermal convection on structural mechanics of the cell, and to exhibit a correlation between velocity fields and mechanical deformation of the steel shell.

Acknowledgements

The authors gratefully acknowledge the support of the Swiss National Science Foundation and the company ALCAN.

References

[1] P. Fellner, G.M. Haarberg, J. Hives, H. Kvande, A. Sterten, J. Thonstad, Aluminium Electrolysis Fundamental of the Hall–Héroult Process, third ed., Aluminium-Verlag, 2001.

[2] K. Grjotheim, H. Kvande, Understanding the Hall–Herlout Process for Production of Aluminium, Aluminium-Verlag, Dusseldorf, 1986.

[3] V. Bojarevics, M. Dupuis, J. Freiberg, Demonstration thermo-electric and MHD mathematical models of a 500 kA Al electrolysis cell, in: COM 42nd Conference of Metallurgists, Vancouver, Canada, 2003.

[4] L. Consiglieri, M.C. Muniz, Existence of solution for a free boundary problem in the thermoelectrical modelling of an aluminium electrolytic cell, European Journal of Applied Mathematics 14 (2003) 201–216.

[5] M.C. Muniz Castineira, Estudio matematico de un problema de Stefan relacionado con la modelizacion termoelectrica de cubas de electrolisis de aluminio, Universidade de Santiago de Compostela, Teses Num 489, 1995.

[6] Y. Safa, Simulation Numérique des phénomènes thermiques et magnétohydrodynamiques dans une cellule de Hall–Héroult, EPFL, Ph.D. thesis No. 3185, 2005.

[7] E.S. Filatov, V.A. Khokhlov, A. Solheim, J. Thonstad, Thermal conductivity in cryolitic melts-new data and its influence on heat transfer in aluminium cells, Light Metals (1998) 501–506.

[8] S.H. Davis, Thermocapillary instabilities, Annual Review of Fluid Mechanics 19 (1987) 403–435.

[9] S. Rolseth, A. Solheim, Some surface and interfacial phenomena encountered in aluminium electrolysis, Light Metals, Norway; 2001, 469–474.

[10] A. Bejan, D.A. Nield, Convection in Porous Media, Springer Verlag, 1992.

[11] A.E. Berger, H. Brezis, J.C.W. Rogers, A numerical method for solving the problem $u_t - \triangle f(u) = 0$; RAIRO numerical analysis 13 (4) (1979) 297–312.

[12] E. Erik, A. Ern, Nonlinear diffusion and discrete maximum principle for stabilized Galerkin approximations of the convection–diffusion-reaction equation, Computer Methods in Applied Mechanics and Engineering 191 (2002) 3833–3855.

[13] L.P. Franca, S.L. Frey, T.J.R. Hughes, Stabilized nite element methods: I. Application to the advective–diffusive model, Computer Methods in Applied Mechanics and Engineering 95 (1992).

[14] M. Dupuis (Génisim Canada), Process simulation, TMS Course on Industrial Aluminum Electrolysis, 1997.

[15] M.V. Romerio, M.A. Secretan, Magnetohydrodynamic equilibrium in aluminium electrolytic cells, Computer Physics Reports 3 (June II) (1986).

[16] J. Descloux, M. Flueck, M.V. Romerio, A modelling of the stability of aluminum electrolysis cells. Nonlinear partial differential equations and their applications, 1998, Collège de France Seminar, vol. XIII, Pitman Research Notes in Mathematics, Series 391.

[17] D. Munger, Simulation numérique des instabilités magnétohydrodynamiques dans les cuves de production de l'aluminium, Département de physique, Université de Montréal, Canada, Master thesis, 2004.

[18] J.F. Gerbeau, Problèmes mathématiques et numériques posés par la modélisation de l'électrolyse de l'aluminium, Ecole Nationale des Ponts et Chaussées, France, Ph.D. thesis, 1998.

[19] M. Dupuis et al., Cathode shell stress modelling, Light Metals (1991) 427–430.

[20] M. Dupuis, I. Tabsh, Evaluations of thermal stresses due to coke preheat of a Hall–Héroult cell, in: Proceeding of the ANSYS®, 6th International Conference, vol. 1, 1994, pp. 3.13–3.23.

[21] G. D'Amours et al., Multi axial mechanical behavior of the carbon cathode: understanding, modelling and identification, Light Metals (2003) 633–639.

[22] M. Flueck, J. Rappaz, Y. Safa, Influence of thermo-hydraulic fields on structural mechanics of aluminum reduction cells, Light Metals (2006) 433–438.